PHYSICS

Superadiabatic population transfer in a three-level superconducting circuit

Antti Vepsäläinen, Sergey Danilin, Gheorghe Sorin Paraoanu*

Adiabatic manipulation of the quantum state is an essential tool in modern quantum information processing. Here, we demonstrate the speedup of the adiabatic population transfer in a three-level superconducting transmon circuit by suppressing the spurious nonadiabatic excitations with an additional two-photon microwave pulse. We apply this superadiabatic method to the stimulated Raman adiabatic passage, realizing fast and robust population transfer from the ground state to the second excited state of the quantum circuit.

INTRODUCTION

The ability to accurately manipulate the state of quantum systems is one of the prerequisites for high-fidelity quantum information processing (*1*). The adiabatic control of quantum states is based on slowly modifying the energy eigenstates of gapped systems; if the condition for adiabatic following is satisfied, the system remains in its instantaneous eigenstate at any moment in time. Techniques that are generically referred to as shortcuts to adiabaticity (*2*) aim at achieving faster operation times through a guided evolution of the system toward the desired final state, bypassing the restriction of the adiabatic theorem.

For adiabatic quantum computing (*3*), quantum annealing (*4*, *5*), and holonomic quantum computing (*6*–*8*), shortcuts to adiabaticity would be one important route to quantum advantage (*9*). In quantum thermodynamics, the suppression of interlevel transitions during adiabatic cycles could lead to engines with increased efficiency (*10*), providing novel insights into the foundations of the third law of thermodynamics (*11*–*13*). Furthermore, in multilevel quantum information processing (*14*), shortcuts to adiabaticity can be used for robust gates (*15*) and efficient initial state preparation.

Superadiabatic protocols (also called transitionless driving) (*16*–*19*) are a type of shortcut to adiabaticity based on counterdiabatic driving—designed such that they suppress nonadiabatic excitations; in consequence, the system follows the instantaneous Hamiltonian eigenstate at any time during evolution. These protocols are universal, and the robustness against errors is inherited from the corresponding adiabatic process. However, a major difficulty in implementing them stems from the fact that the superadiabatic control drive uses complex couplings with externally controlled and stable Peierls phases (*20*). In optical setups, this would require lasers with exquisitely low phase noise. This is why so far superadiabatic protocols have been demonstrated only in simple configurations, involving either two levels (*21*, *22*) or two control fields (*23*–*25*).

Here, we show that the required phase stability can be achieved in the microwave regime using circuit quantum electrodynamics as the experimental platform (*26*). We use the first three states of a superconducting transmon circuit (*27*) to transfer population between the ground state and the second excited state. This is an important task in quantum control of multilevel systems, where fast and efficient state preparation serves as an initial step for many algorithms (*28*, *29*). We achieve this by using three microwave pulses: Two of them realize the stimulated Raman adiabatic passage (STIRAP) (*30*–*32*), while the third is a two-photon process creating the counterdiabatic Hamiltonian, which forces the system to follow its instantaneous eigenstate even though the adiabatic condition is violated. This type of driving, called loop configuration (*33*), results in an externally controlled gauge-invariant phase and implements the superadiabatic STIRAP (saSTIRAP) protocol (*34*, *35*).

For a three-level system in the ladder configuration, the resonant STIRAP Hamiltonian can be written as

$$H_0(t) = \frac{\hbar}{2}\left[\Omega_{01}(t)e^{i\phi_{01}}|0\rangle\langle 1| + \Omega_{12}(t)e^{i\phi_{12}}|1\rangle\langle 2| + \text{h.c.}\right] \quad (1)$$

where $\Omega_{01}(t)$ and $\Omega_{12}(t)$ describe the Rabi coupling of the microwave drive pulses to the transmon in the frame rotating with the drive frequencies. The drives have a Gaussian shape (*32*)

$$\Omega_{01}(t) = \Omega_{01}\exp[-t^2/(2\sigma^2)],$$
$$\Omega_{12}(t) = \Omega_{12}\exp[-(t-t_s)^2/(2\sigma^2)] \quad (2)$$

where t_s is the lag between the two pulses. In the experiment, we use two intermediate frequency microwave tones with externally controlled phases, ϕ_{01} and ϕ_{12}, which are digitally mixed with the pulse envelopes $\Omega_{01}(t)$ and $\Omega_{12}(t)$ using an arbitrary waveform generator (see the Supplementary Materials for details). The pulses are further mixed in an analog IQ mixer with a local oscillator tone $\omega_{LO}/(2\pi) = 6.92$ GHz to produce two signals that resonantly drive the 0–1 and 1–2 transitions of the three-level system at frequencies $\omega_{01}/(2\pi) = 6.99$ GHz and $\omega_{12}/(2\pi) = 6.62$ GHz (see Fig. 1).

In the STIRAP protocol, the system follows adiabatically one of the instantaneous eigenstates of the above Hamiltonian, called the dark state, $|D(t)\rangle = \cos\Theta(t)e^{i\phi_{12}}|0\rangle - \sin\Theta(t)e^{-i\phi_{01}}|2\rangle$, where $\Theta(t) = \tan^{-1}[\Omega_{01}(t)/\Omega_{12}(t)]$ changes slowly from 0 to $\pi/2$. This implies that the pulse driving the 1–2 transition is counterintuitively applied before the 0–1 pulse, enabling the population to be transferred directly to the second excited state without exciting the intermediate state $|1\rangle$ at any time in between. However, if the change in the amplitudes of the control signals is too abrupt, the system gets diabatically excited away from the state $|D(t)\rangle$, reducing the transferred population and therefore limiting the fidelity of the process.

The spurious excitations of STIRAP can be canceled using the superadiabatic method (*16*–*19*). The idea is to design a new control Hamiltonian, which evolves the system through the adiabatic states given by the STIRAP Hamiltonian in Eq. 1, even when the adiabatic condition is not fully satisfied (*16*). The form of the counterdiabatic Hamiltonian can be

Low Temperature Laboratory, Department of Applied Physics, Aalto University School of Science, P.O. Box 15100, FI-00076 AALTO, Finland.
*Corresponding author. Email: sorin.paraoanu@aalto.fi

found by reverse Hamiltonian engineering (*19*, *34*, *35*) (see the Supplementary Materials for the derivation), requiring the addition of a third control pulse given by

$$H_{cd}(t) = \frac{\hbar}{2}\left[\Omega_{02}(t)e^{-i\phi_{20}}|0\rangle\langle 2| + \text{h.c.}\right] \quad (3)$$

with Rabi coupling

$$\Omega_{02}(t) = 2\dot{\Theta}(t) \quad (4)$$

and a phase ϕ_{20} that must satisfy the relation $\phi_{01} + \phi_{12} + \phi_{20} = -\pi/2$ (*36*). For the STIRAP pulse amplitudes given in Eq. 2 and assuming $\Omega_{01} = \Omega_{12}$, the shape of the counterdiabatic pulse can be evaluated as (*35*)

$$\Omega_{02}(t) = -\frac{t_s}{\sigma^2}\frac{1}{\cosh\left[-\frac{t_s}{\sigma^2}(t - t_s/2)\right]} \quad (5)$$

To experimentally create the microwave pulse implementing the counterdiabatic Hamiltonian, we use a two-photon process generated by a third microwave drive field with frequency $\omega_{2ph} = (\omega_{01} + \omega_{12})/2$ and phase ϕ_{2ph}, which couples into the 0–1 and 1–2 transitions with respective Rabi couplings Ω_{2ph} and $\sqrt{2}\Omega_{2ph}$. The factor $\sqrt{2}$ is a consequence of the almost harmonic energy level structure of the transmon circuit, which results in a higher dipole coupling for higher transitions (*27*). The low anharmonicity also leads to selection rules that prevent us from using a direct 0–2 drive to implement the counterdiabatic Hamiltonian. The chosen drive frequency results in detunings $\pm\Delta$ from both the 0–1 and 1–2 transitions, $\Delta = \omega_{01} - \omega_{2ph} = (\omega_{01} - \omega_{12})/2$, thus satisfying the two-photon resonance condition. The two-photon driving generates an effective Rabi coupling $\Omega_{02}(t) = \sqrt{2}\Omega_{2ph}^2/(2\Delta)$ and phase $\phi_{20} = -2\phi_{2ph} - \pi$, which can be obtained from perturbation theory (*15*, *37*). In addition, two-photon driving creates small ac-Stark shifts to all the energy levels, which appear as dynamic detunings of the drive frequencies from the transitions. We compensate for this effect by slightly tuning the phases of all the drive pulses during the evolution (see Methods for details).

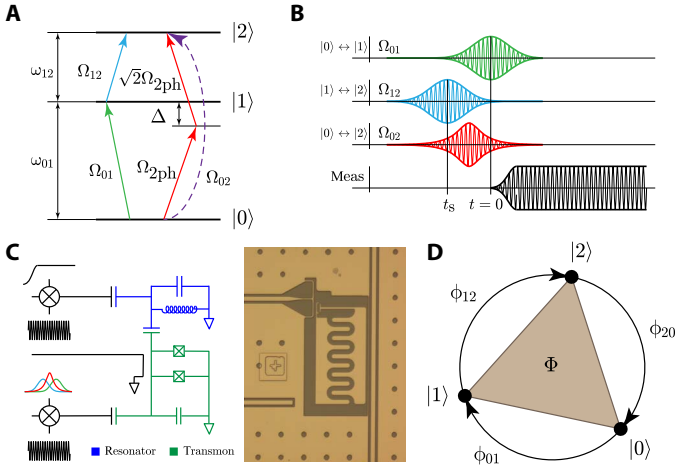

Fig. 1. Schematic of the experiment. (**A**) Loop driving for saSTIRAP: A counterdiabatic drive with effective Rabi frequency Ω_{02} (dashed purple arrow) is applied in parallel with a STIRAP sequence consisting of pulses Ω_{01} and Ω_{12}, which are resonant with the respective transitions 0–1 and 1–2. The counterdiabatic drive is a two-photon process realized by an off-resonant pulse (detuning Δ with respect to the first transition), which couples with strengths Ω_{2ph} and $\sqrt{2}\Omega_{2ph}$ into the corresponding transitions. (**B**) Schematic of the timings and shapes of the pulses. The last pulse is the measurement pulse applied to the resonator. (**C**) Schematic (including the IQ mixers used for driving and measurement) and optical image of the transmon. (**D**) Geometric representation of the Hamiltonian on a three-site plaquette with Peierls hopping and resulting gauge-invariant phase $\Phi = \phi_{01} + \phi_{12} + \phi_{20}$.

RESULTS

Efficient transfer of population

To demonstrate that the superadiabatic protocol corrects for the nonadiabatic losses even when the adiabaticity condition for STIRAP is not satisfied, we experimentally compare the two methods in Fig. 2. Here, the peak STIRAP amplitudes Ω_{01} and Ω_{12} were chosen as $\Omega_{01}/(2\pi) = \Omega_{12}/(2\pi) = 25.5$ MHz, the separation of the two STIRAP pulses is $t_s/\sigma = -1.5$, and the widths of the Gaussian pulse shapes are $\sigma = 20$ ns. During STIRAP, there is a significant population in state $|1\rangle$ due to the violation of the adiabatic condition, which results in transitions between the instantaneous eigenstates of the system. Consequently, the population p_2 is only 0.8 after the pulses. In the saSTIRAP experiment, there is almost no population in state $|1\rangle$ and p_2 reaches 0.96, which is very close to the ideal performance, demonstrating the power of the superadiabatic method. The result is supported by the numerical simulation, shown with solid lines (see Methods for details). The dashed lines show a simulation with the same parameters but without decoherence, resulting in $p_2 = 0.9997$ and confirming that most of the remaining losses in the saSTIRAP experiment are caused by the energy relaxation of the qutrit (with rates $\Gamma_{01} = 0.6$ MHz and $\Gamma_{12} = 0.83$ MHz, obtained by independent measurements).

In Fig. 3, we show the performance of the superadiabatic protocol for a wide range of STIRAP parameters. We explore the parameter space (t_s, σ) by varying the STIRAP pulse width σ and the normalized STIRAP pulse separation $|t_s|/\sigma$, as shown in Fig. 3A. The optimal pulse separation for STIRAP is $t_s/\sigma = -1.5$ (*31*). In the upper part of the plot, the STIRAP fidelity is low because the separation of the pulses

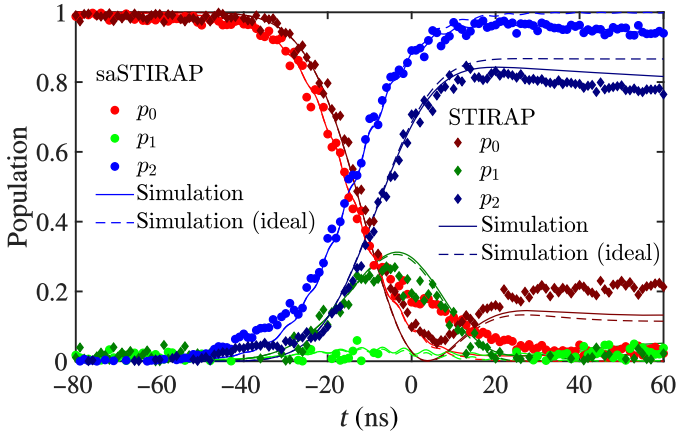

Fig. 2. Comparison between STIRAP and saSTIRAP. Time evolution of the populations p_0, p_1, and p_2 during STIRAP (diamonds) and saSTIRAP (circles). The solid lines show the corresponding simulation, which includes decoherence. A simulation for the ideal case without decoherence is presented with dashed lines. The experiment was performed with the parameters $\Omega_{01} = \Omega_{12} = 25.5$ MHz, $t_s/\sigma = -1.5$, and $\sigma = 20$ ns.

is too large, whereas for small σ the adiabatic condition is not satisfied. STIRAP also fails for too small pulse separations; some high-fidelity population transfer seen around $t_s = 0$ in the experiment is not due to STIRAP but is driven by the holonomic gate studied in (*8*, *38*). The experiment can be compared to a numerical simulation, which replicates the results accurately (right panel in the figure). Figure 3B demonstrates that, by adding the counterdiabatic drive, we are able to counteract the diabatic losses for almost all the STIRAP parameters.

The performance of the protocol can be further characterized by comparing its transfer speed to the quantum speed limit at the maximum counter-diabatic pulse coupling. We follow a convention where the duration of the saSTIRAP protocol is defined as the time lapse between an initial state with population 0.99 in the ground state and a final state with population 0.9 in the second excited state (*35*). This corresponds to initial and final mixing angles of $\Theta_i = 0.03\ \pi$ and $\Theta_f = 0.4\ \pi$, respectively. For calculating the quantum speed limit, we use the Bhattacharyya bound (*39*) for the two-level subspace spanned by the states $|0\rangle$ and $|2\rangle$ under the maximal experimentally accessible two-photon Rabi drive $\Omega_{02}^{\max}/(2\pi) = 48$ MHz. We take the initial and final states with the same populations as above, which results in $T_{\mathrm{QSL}}^{0.9} = 2\arccos|\langle D(\theta_i)|D(\theta_f)\rangle|/\Omega_{02}^{\max} \approx 7.7$ ns. The quantum speed limit can be compared to the transfer times for the saSTIRAP protocol, which are shown by the overlaid solid lines in Fig. 3B. The transfer times are the fastest ($T_{\mathrm{saSTIRAP}} \approx 2.0 T_{\mathrm{QSL}}$) in the upper left corner of the panels corresponding to σ = 10 ns and $|t_s/\sigma| = 3$. However, as we approach that point, the STIRAP fidelity is also reduced and, in consequence, the population transfer occurs predominantly due to the counterdiabatic driving. Thus, the population transfer will start to be increasingly sensitive to the amplitudes of the pulses. To improve the robustness, the strength of the STIRAP part must be increased by reducing t_s/σ or by increasing σ, which leads to a reduction of transfer speed. The trade-off is important for the potential applications of the superadiabatic method and will be analyzed later in greater detail.

Gauge-invariant phase

Loop driving with complex couplings between each pair of states results in a nontrivial synthetic gauge structure on the triangular plaquette formed by the three states, previously studied theoretically in (*36*, *40*); related schemes have been proposed for cold atom lattices in (*41*). See Fig. 1D for a simple illustration.

In Fig. 4, we demonstrate experimentally that, in a three-level transmon, the dynamics of the system is determined by the gauge-invariant phase $\Phi = \phi_{01} + \phi_{12} + \phi_{20}$. We present the population transferred to state $|2\rangle$, when one of the phases ϕ_{01}, ϕ_{12}, or ϕ_{2ph} is kept fixed, while the other two are varied. The populations are measured at a time $t = 20$ ns after the maximum of the 0–1 drive pulse, and the two-photon pulse is set to satisfy Eq. 4. The experiment shows that the transferred population to state $|2\rangle$, p_2, depends only on $\phi_{01} + \phi_{12} + \phi_{20} = \Phi$ and not on each phase separately (*36*). This allows us to choose the gauge $\phi_{01} = \phi_{12} = 0$ and use $\phi_{20} = \Phi = -2\phi_{2ph} - \pi$ as the externally controlled gauge-invariant phase.

In this gauge, the full Hamiltonian of the system reads

$$H(t) = \frac{\hbar}{2}[\Omega_{01}(t)|0\rangle\langle 1| + \Omega_{12}(t)|1\rangle\langle 2| + \Omega_{02}(t)e^{-i\Phi}|0\rangle\langle 2| + \mathrm{h.c.}] \quad (6)$$

thus simplifying the problem significantly (see also the Supplementary Materials).

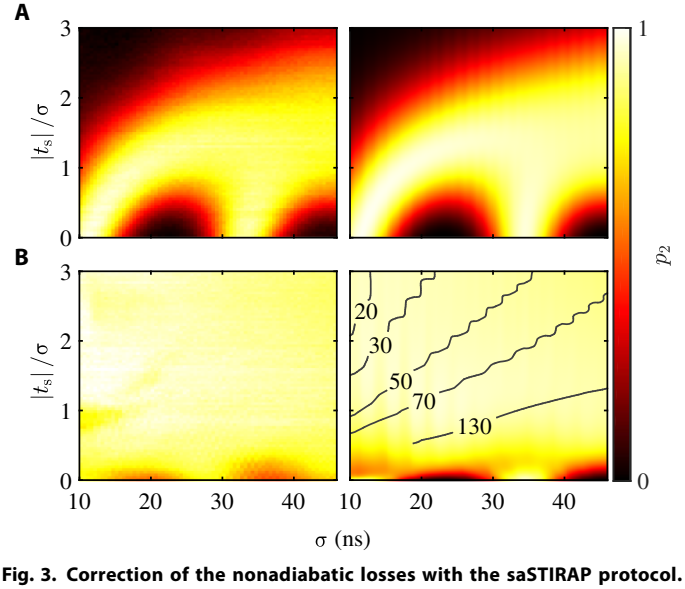

Fig. 3. Correction of the nonadiabatic losses with the saSTIRAP protocol. (**A**) Population p_2 in the state $|2\rangle$ for the STIRAP process with $\Omega_{01}/(2\pi) = \Omega_{12}/(2\pi) = 25.5$ MHz as a function of the pulse width σ and the normalized pulse separation $|t_s|/\sigma$. (**B**) Population p_2 for the corresponding saSTIRAP process. The left plots are experiments, while the right ones are the corresponding simulation results. The solid black lines show the transfer time $t_{\mathrm{tr}}^{0.9}$ in nanoseconds to achieve the population $p_2 = 0.9$ in saSTIRAP.

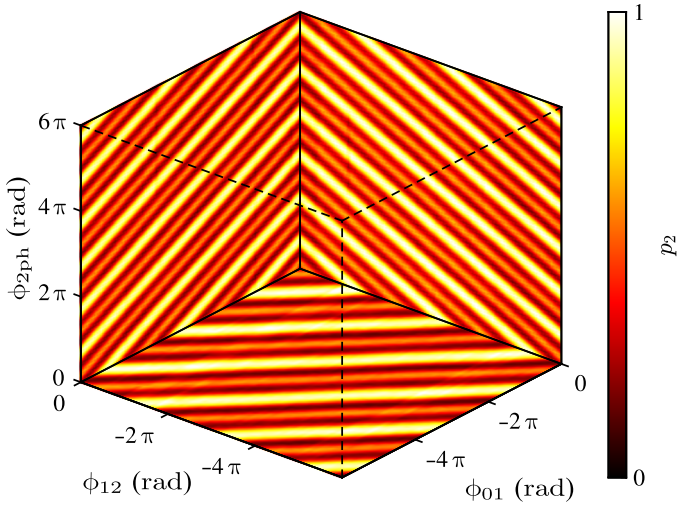

Fig. 4. Control of the system dynamics with the gauge-invariant phase. Under loop driving, the phase Φ is a gauge-invariant quantity, in analogy with lattice gauge theories, where it is typically produced by an applied magnetic field. The three-dimensional plot shows lines of constant population p_2 in the state $|2\rangle$, in the orthogonal planes (ϕ_{12}, ϕ_{2ph}) (with ϕ_{01} constant), (ϕ_{01}, ϕ_{2ph}) (with ϕ_{12} constant), and (ϕ_{12}, ϕ_{01}) (with ϕ_{2ph} constant). The gauge-invariance relation $\phi_{01} + \phi_{12} - 2\phi_{2ph} - \pi = \Phi$ corresponds to tilted planes that intersect the axes. Note also that the periodicity along the ϕ_{2ph} axis is twice that of the periodicity along the axes ϕ_{01} and ϕ_{12} as a result of two-photon driving. In the experiment, we had $\Omega_{01}/(2\pi) = \Omega_{12}/(2\pi) = 25.5$ MHz, $t_s = -30$ ns, and σ = 20 ns.

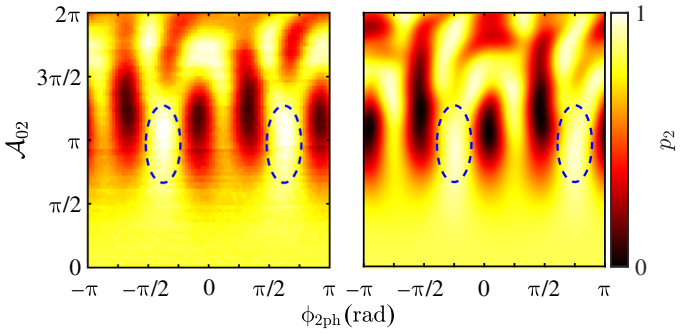

Fig. 5. Robustness of saSTIRAP against variations in the counterdiabatic pulse parameters. Population p_2 in the state $|2\rangle$ as a function of the area of the counterdiabatic pulse and the gauge-invariant phase. The experimental result is shown in the left panel with the corresponding simulation in the right panel. The parameters used in the experiment are $t_s = -30$ ns, $\sigma = 20$ ns, and $\mathcal{A} = 4.2\pi$. Note that $\mathcal{A}_{02} = 0$ corresponds to pure STIRAP. The blue dashed-line ellipses represent the areas where saSTIRAP is robust against changes in parameters $\mathcal{A}_{02}$ and ϕ_{2ph}.

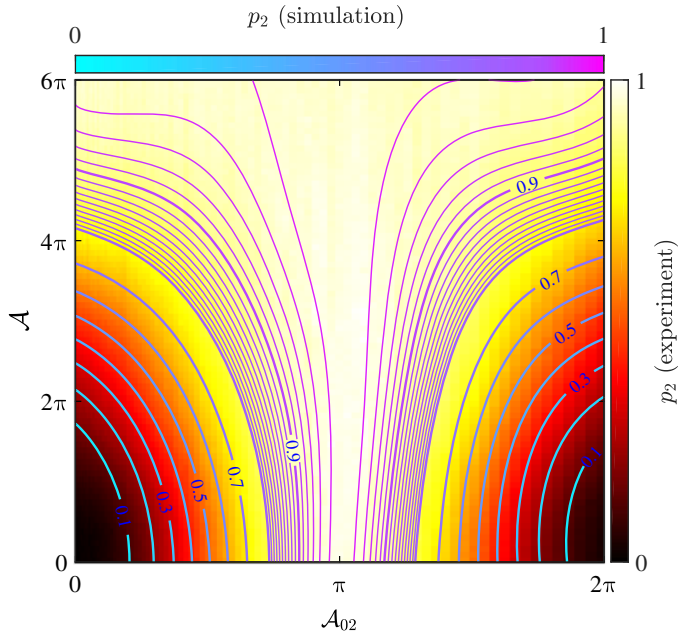

Fig. 6. Comparison between saSTIRAP and nonadiabatic population transfer. Transferred population p_2 (experiment) as a function of the STIRAP pulse area $\mathcal{A}$ defined in Eq. 8 and the two-photon pulse area $\mathcal{A}_{02}$ from Eq. 7. We also show isopopulation lines (from 0.1 to 0.8 in steps of 0.1 and from 0.8 to 1.0 in steps of 0.01) obtained from the simulations, showing agreement with the data and delineating the same region of high transfer as that obtained from the experiment. In this experiment, the peak STIRAP Rabi frequencies were increased from zero to $\Omega_{01}/(2\pi) = \Omega_{12}/(2\pi) = 40$ MHz. Similarly, the two-photon pulse amplitude was varied from zero to $\Omega_{2ph}/(2\pi) = 77$ MHz. The horizontal axis with $\mathcal{A} = 0$ corresponds to two-photon Rabi driving, whereas the vertical axis with $\mathcal{A}_{02} = 0$ corresponds to standard STIRAP. In the experiment, the STIRAP pulse separation was $t_s = -30$ ns and the pulse width was $\sigma = 20$ ns.

Robustness properties

STIRAP is known to be insensitive to changes in the amplitudes of the drive fields. The crucial question is whether this robustness extends to the amplitude of the counterdiabatic field, as for the practical applications of the protocol its resilience to errors is a critical feature distinguishing it from the nonadiabatic methods. First, we introduce the area of the counterdiabatic pulse

$$\mathcal{A}_{02} = \int_{-\infty}^{\infty} dt \Omega_{02}(t) \tag{7}$$

and we define STIRAP pulse area as

$$\mathcal{A} = \int_{-\infty}^{\infty} dt \sqrt{\Omega_{01}^2(t) + \Omega_{12}^2(t)} \tag{8}$$

which is the measure of adiabaticity of STIRAP according to the global adiabatic condition $\mathcal{A} \gg \pi/2$ (*31*). In Fig. 5, we show the population of state $|2\rangle$, p_2, as a function of the counterdiabatic pulse area and its phase. The saSTIRAP process reveals its useful properties for the parameter values inside the area outlined with blue dashed-line ellipses, where the pulse areas $\mathcal{A}_{02}$ are close to π, as expected from Eq. 5. For the parameters $(\mathcal{A}_{02}, \phi_{2ph})$ inside the ellipses, p_2 is a rather slow-varying function of $\mathcal{A}_{02}$, indicating that saSTIRAP is robust against errors in the area of the counterdiabatic pulse. In contrast, population transfer can also take place for values $(\mathcal{A}_{02}, \phi_{2ph})$ outside the ellipses, but without robustness against variations of $\mathcal{A}_{02}$. The right panel shows a corresponding numerical simulation, which matches the pattern seen in the experiment quite well. From the simulation, we can also see that the maximum transfer occurs around an optimal phase, which is very close to the ideal $\phi_{2ph} = -\pi/4 + n\pi$. In the experiment, a small shift exists in the phases due to the phase imbalance of the IQ mixer (see Fig. 1C) used to combine the driving pulses (more details available in the Supplementary Materials).

To explicitly compare saSTIRAP with the direct nonadiabatic process, we show in Fig. 6 the transferred population as a function of the area $\mathcal{A}$ of the STIRAP pulses and $\mathcal{A}_{02}$ of the counterdiabatic pulse. The phase ϕ_{2ph} is tuned to yield the maximum population in state $|2\rangle$ at each value of the STIRAP area $\mathcal{A}$. In the presence of only the counterdiabatic pulse (along the horizontal axis where $\mathcal{A} = 0$), the population transfer, as expected, occurs in a rather narrow range of $\mathcal{A}_{02}$ values around π. When the area of the STIRAP pulses is increased (at approximately $\mathcal{A} \approx 2\pi$), the range of values of $\mathcal{A}_{02}$ where the transfer occurs enlarges significantly. This demonstrates the advantage that the superadiabatic method offers: It has better fidelity than STIRAP while being less sensitive to the variation in $\mathcal{A}_{02}$ than a raw π pulse. Theoretically, the fidelity of STIRAP approaches unity only in the limit of infinite pulse area (the adiabatic condition is fully satisfied), whereas ideal saSTIRAP has unit fidelity for all the values of the STIRAP pulse area.

Figure 6 also demonstrates that, even though the maximal effective two-photon coupling is smaller than the direct 0–1 and 1–2 couplings, it does not severely restrict the speed of the method, because the optimal two-photon pulse area $\mathcal{A}_{02} = \pi$ is usually significantly smaller than the STIRAP area $\mathcal{A}$ required to provide the demanded robustness. This is also an advantage over rapid adiabatic passage (*42*, *43*), where a much stronger two-photon pulse on the 0–2 transition would be needed.

METHODS

Three-level quantum tomography

The state of the qutrit was obtained by three-level quantum tomography, where the diagonal elements of the density matrix were calculated

from the averaged IQ traces of the cavity response (*44*). The measured trace

$$r_{\mathrm{meas}}(\tau) = \sum_{i=0,1,2} p_i r_i(\tau) \tag{9}$$

is a linear combination of calibration traces corresponding to states $|0\rangle$, $|1\rangle$, and $|2\rangle$ with weight factors p_0, p_1, and p_2, which give the occupation probability of each state. Here, τ is the time from the beginning of the measurement pulse. Using the least squares fit of the calibration traces to the measured trace, we can extract the most likely occupation probabilities for the three-level system.

The calibration traces inevitably include the effect of relaxation, which, if left uncompensated, can lead to an artificial overestimation of the state population in both STIRAP and saSTIRAP. However, since we know the relaxation rates, we can correct for this effect by modifying the calibration trajectories to include some contribution from the lower states, described by errors ζ_{ij} with $i < j$. The measured trajectory r_j is then given by

$$r_j(\tau) = \left(1 - \sum_{i<j}\zeta_{ij}\right)\tilde{r}_j(\tau) + \sum_{i<j}\zeta_{ij}\tilde{r}_i(\tau) \tag{10}$$

with $\tilde{r}_i(\tau)$ describing the unknown ideal responses of state $|i\rangle$. From the above equation, the ideal responses can be solved iteratively, yielding

$$\begin{aligned}
\tilde{r}_0(\tau) &= r_0(\tau),\\
\tilde{r}_1(\tau) &= \frac{r_1(\tau) - \zeta_{01}\tilde{r}_0(\tau)}{1 - \zeta_{01}},\\
\tilde{r}_2(\tau) &= \frac{r_2(\tau) - \zeta_{02}\tilde{r}_0(\tau) - \zeta_{12}\tilde{r}_1(\tau)}{1 - \zeta_{02} - \zeta_{12}}
\end{aligned} \tag{11}$$

We used $\zeta_{01} = 0.01$, $\zeta_{12} = 0.01$, and $\zeta_{02} = 0.02$, which are obtained by comparing a reference Rabi experiment to a corresponding simulation with known energy relaxation rates.

Dynamical phase correction

The off-resonant two-photon driving produced parasitic ac-Stark shifts of the energy levels, which we compensated for by using dynamically adjusted phases. Following (*15*), the ac-Stark shifts can be calculated from the second-order perturbation theory as $\tilde{E}_n(t) = E_n + \langle n|V(t)|n\rangle + \sum_{k\neq n}\frac{\langle k|V(t)|n\rangle}{E_n - E_k}$, where $V(t)$ consists of the off-diagonal elements of the two-photon drive Hamiltonian $V = \hbar\Omega_{2\mathrm{ph}}(t)(|0\rangle\langle 1|e^{i\phi_{2\mathrm{ph}}} + \sqrt{2}|1\rangle\langle 2|e^{i\phi_{2\mathrm{ph}}} + \mathrm{h.c.})/2$ in the frame rotating with the drive. The energies E_n are the detunings of the drive from the 0–1 and 1–2 transitions, $E_0 = 0$, $E_1 = \hbar\Delta$, and $E_2 = 0$. The resulting ac-Stark shifts $\varepsilon_{n,k} = \tilde{E}_k - \tilde{E}_n - (E_k - E_n)$ are $\varepsilon_{01}(t) = \hbar|\Omega_{2\mathrm{ph}}|^2/\Delta$, $\varepsilon_{12} = -5\hbar|\Omega_{2\mathrm{ph}}|^2/(4\Delta)$, and $\varepsilon_{0,2} = -\hbar|\Omega_{2\mathrm{ph}}|^2/(4\Delta)$. To compensate for the shifts in the energy levels, we dynamically modified the phases of all the three drives as $\phi_{nk}(t) \rightarrow \phi_{nk} + \int_{-\infty}^{t} d\tau\varepsilon_{nk}(\tau)/\hbar$. As a result, the frequencies of the drives matched the ac-Stark shifted qutrit transition frequencies at all instants of time.

Numerical simulations

The system was modeled with the Hamiltonian

$$\begin{aligned}
H_{\mathrm{sim}}(t) = H_0 + \hbar\Omega_{2\mathrm{ph}}(t)/2\big(&|0\rangle\langle 1|e^{i(\phi_{2\mathrm{ph}}(t) - \Delta t)}\\
&+ \sqrt{2}|1\rangle\langle 2|e^{i(\phi_{2\mathrm{ph}}(t) + \Delta t)} + \mathrm{h.c.}\big)
\end{aligned} \tag{12}$$

in the frame rotating with the STIRAP drives. Here, H_0 is the STIRAP Hamiltonian given in Eq. 1, and the evolution of the system was solved from the Lindblad master equation $\dot{\rho}(t) = -i[H_{\mathrm{sim}}(t), \rho(t)]/\hbar + \Sigma_{i=0,1}\Gamma_{i,i+1}(|i\rangle\langle i+1|\rho(t)|i+1\rangle\langle i| - \frac{1}{2}(|i\rangle\langle i|\rho(t) + \rho(t)|i\rangle\langle i|))$, where $\rho(t)$ is the density matrix of the system and $\Gamma_{i,i+1}$ are the energy relaxation rates (obtained by independent qubit characterization measurements).

CONCLUSIONS

We have demonstrated a speedup of population transfer in STIRAP by introducing an additional counterdiabatic two-photon control pulse that corrects for nonadiabaticity. The process was controlled by the pulse amplitudes and by a gauge-invariant phase. We have characterized the robustness of the process with respect to the counterdiabatic field and evaluated the trade-off between the speed of the process and the insensitivity to control parameters.

SUPPLEMENTARY MATERIALS

Supplementary material for this article is available at http://advances.sciencemag.org/cgi/content/full/5/2/eaau5999/DC1

Experimental setup and sample
Reverse engineering of the counteradiabatic drive
Synthetic Peierls couplings on the triangular plaquette
Fig. S1. Electronics, cryogenics, and sample schematic.
Fig. S2. Pulse sequence for saSTIRAP.
References (*45*–*47*)

REFERENCES AND NOTES

1. D. P. DiVincenzo, The physical implementation of quantum computation. arXiv:quant-ph/0002077 (25 February 2000).
2. E. Torrontegui, S. Ibáñez, S. Martínez-Garaot, M. Modugno, A. del Campo, D. Guéry-Odelin, A. Ruschhaupt, X. Chen, J. G. Muga, Shortcuts to adiabaticity, in *Advances in Atomic, Molecular, and Optical Physics*, P. R. B. Ennio Arimondo, C. C. Lin, Eds. (Academic Press, 2013), vol. 62, pp. 117–169.
3. E. Farhi, J. Goldstone, S. Gutmann, J. Lapan, A. Lundgren, D. Preda, A quantum adiabatic evolution algorithm applied to random instances of an NP-complete problem. *Science* **292**, 472–475 (2001).
4. A. Das, B. K. Chakrabarti, *Colloquium*: Quantum annealing and analog quantum computation. *Rev. Mod. Phys.* **80**, 1061–1081 (2008).
5. M. W. Johnson, M. H. S. Amin, S. Gildert, T. Lanting, F. Hamze, N. Dickson, R. Harris, A. J. Berkley, J. Johansson, P. Bunyk, E. M. Chapple, C. Enderud, J. P. Hilton, K. Karimi, E. Ladizinsky, N. Ladizinsky, T. Oh, I. Perminov, C. Rich, M. C. Thom, E. Tolkacheva, C. J. S. Truncik, S. Uchaikin, J. Wang, B. Wilson, G. Rose, Quantum annealing with manufactured spins. *Nature* **473**, 194–198 (2011).
6. E. Sjöqvist, D. M. Tong, L. M. Andersson, B. Hessmo, M. Johansson, K. Singh, Non-adiabatic holonomic quantum computation. *New J. Phys.* **14**, 103035 (2012).
7. P. Zanardi, M. Rasetti, Holonomic quantum computation. *Phys. Lett. A* **264**, 94–99 (1999).
8. A. A. Abdumalikov Jr., J. M. Fink, K. Juliusson, M. Pechal, S. Berger, A. Wallraff, S. Filipp, Experimental realization of non-Abelian non-adiabatic geometric gates. *Nature* **496**, 482–485 (2013).
9. S. Boixo, T. F. Rønnow, S. V. Isakov, Z. Wang, D. Wecker, D. A. Lidar, J. M. Martinis, M. Troyer, Evidence for quantum annealing with more than one hundred qubits. *Nat. Phys.* **10**, 218–224 (2014).
10. A. del Campo, J. Goold, M. Paternostro, More bang for your buck: Super-adiabatic quantum engines. *Sci. Rep.* **4**, 6208 (2014).
11. X. Chen, J. G. Muga, Transient energy excitation in shortcuts to adiabaticity for the time-dependent harmonic oscillator. *Phys. Rev. A* **82**, 053403 (2010).
12. P. Salamon, K. H. Hoffmann, Y. Rezek, R. Kosloff, Maximum work in minimum time from a conservative quantum system. *Phys. Chem. Chem. Phys.* **11**, 1027–1032 (2009).
13. Y. Rezek, P. Salamon, K. H. Hoffmann, R. Kosloff, The quantum refrigerator: The quest for absolute zero. *Europhys. Lett.* **85**, 30008 (2009).
14. B. P. Lanyon, M. Barbieri, M. P. Almeida, T. Jennewein, T. C. Ralph, K. J. Resch, G. J. Pryde, J. L. O'Brien, A. Gilchrist, A. G. White, Simplifying quantum logic using higher-dimensional Hilbert spaces. *Nat. Phys.* **5**, 134–140 (2009).
15. A. Vepsäläinen, S. Danilin, G. S. Paraoanu, Optimal superadiabatic population transfer and gates by dynamical phase corrections. *Quantum Sci. Technol.* **3**, 024006 (2018).

16. M. Demirplak, S. A. Rice, Adiabatic population transfer with control fields. *J. Phys. Chem. A* **107**, 9937–9945 (2003).
17. M. Demirplak, S. A. Rice, Assisted adiabatic passage revisited. *J. Phys. Chem. B* **109**, 6838–6844 (2005).
18. M. Demirplak, S. A. Rice, On the consistency, extremal, and global properties of counterdiabatic fields. *J. Chem. Phys.* **129**, 154111 (2008).
19. M. V. Berry, Transitionless quantum driving. *J. Phys. A Math. Theor.* **42**, 365303 (2009).
20. R. Peierls, Zur theorie des diamagnetismus von leitungselektronen. *Z. Phys.* **80**, 763–791 (1933).
21. M. G. Bason, M. Viteau, N. Malossi, P. Huillery, E. Arimondo, D. Ciampini, R. Fazio, V. Giovannetti, R. Mannella, O. Morsch, High-fidelity quantum driving. *Nat. Phys.* **8**, 147–152 (2012).
22. J. Zhang, J. H. Shim, I. Niemeyer, T. Taniguchi, T. Teraji, H. Abe, S. Onoda, T. Yamamoto, T. Ohshima, J. Isoya, D. Suter, Experimental implementation of assisted quantum adiabatic passage in a single spin. *Phys. Rev. Lett.* **110**, 240501 (2013).
23. S. An, D. Lv, A. del Campo, K. Kim, Shortcuts to adiabaticity by counterdiabatic driving for trapped-ion displacement in phase space. *Nat. Commun.* **7**, 12999 (2016).
24. Y.-X. Du, Z.-T. Liang, Y.-C. Li, X.-X. Yue, Q.-X. Lv, W. Huang, X. Chen, H. Yan, S.-L. Zhu, Experimental realization of stimulated Raman shortcut-to-adiabatic passage with cold atoms. *Nat. Commun.* **7**, 12479 (2016).
25. B. B. Zhou, A. Baksic, H. Ribeiro, C. G. Yale, F. J. Heremans, P. C. Jerger, A. Auer, G. Burkard, A. A. Clerk, D. D. Awschalom, Accelerated quantum control using superadiabatic dynamics in a solid-state lambda system. *Nat. Phys.* **13**, 330–334 (2017).
26. A. Wallraff, D. I. Schuster, A. Blais, L. Frunzio, R.-S. Huang, J. Majer, S. Kumar, S. M. Girvin, R. J. Schoelkopf, Strong coupling of a single photon to a superconducting qubit using circuit quantum electrodynamics. *Nature* **431**, 162–167 (2004).
27. J. Koch, T. M. Yu, J. Gambetta, A. A. Houck, D. I. Schuster, J. Majer, A. Blais, M. H. Devoret, S. M. Girvin, R. J. Schoelkopf, Charge-insensitive qubit design derived from the Cooper pair box. *Phys. Rev. A* **76**, 042319 (2007).
28. P. Magnard, P. Kurpiers, B. Royer, T. Walter, J.-C. Besse, S. Gasparinetti, M. Pechal, J. Heinsoo, S. Storz, A. Blais, A. Wallraff, Fast and unconditional all-microwave reset of a superconducting qubit. *Phys. Rev. Lett.* **121**, 060502 (2018).
29. Y. Liu, D. Lan, X. Tan, J. Zhao, P. Zhao, M. Li, K. Zhang, K. Dai, Z. Li, Q. Liu, S. Huang, G. Xue, P. Xu, H. Yu, S.-L. Zhu, Y. Yu, Realization of dark state in a three-dimensional transmon superconducting qutrit. *Appl. Phys. Lett.* **107**, 202601 (2015).
30. U. Gaubatz, P. Rudecki, S. Schiemann, K. Bergmann, Population transfer between molecular vibrational levels by stimulated Raman scattering with partially overlapping laser fields. A new concept and experimental results. *J. Chem. Phys.* **92**, 5363–5376 (1990).
31. N. V. Vitanov, A. A. Rangelov, B. W. Shore, K. Bergmann, Stimulated Raman adiabatic passage in physics, chemistry, and beyond. *Rev. Mod. Phys.* **89**, 015006 (2017).
32. K. S. Kumar, A. Vepsäläinen, S. Danilin, G. S. Paraoanu, Stimulated Raman adiabatic passage in a three-level superconducting circuit. *Nat. Commun.* **7**, 10628 (2016).
33. R. G. Unanyan, L. P. Yatsenko, K. Bergmann, B. W. Shore, Laser-induced adiabatic atomic reorientation with control of diabatic losses. *Opt. Commun.* **139**, 48–54 (1997).
34. X. Chen, I. Lizuain, A. Ruschhaupt, D. Guéry-Odelin, J. G. Muga, Shortcut to adiabatic passage in two- and three-level atoms. *Phys. Rev. Lett.* **105**, 123003 (2010).
35. L. Giannelli, E. Arimondo, Three-level superadiabatic quantum driving. *Phys. Rev. A* **89**, 033419 (2014).
36. A. Benseny, A. Kiely, Y. Zhang, T. Busch, A. Ruschhaupt, Spatial non-adiabatic passage using geometric phases. *EPJ Quantum Technol.* **4**, 3 (2017).
37. D. F. James, J. Jerke, Effective Hamiltonian theory and its applications in quantum information. *Can. J. Phys.* **85**, 625–632 (2007).
38. S. Danilin, A. Vepsäläinen, G. S. Paraoanu, Experimental state control by fast non-Abelian holonomic gates with a superconducting qutrit. *Phys. Scr.* **93**, 055101 (2018).
39. K. Bhattacharyya, Quantum decay and the Mandelstam-Tamm-energy inequality. *J. Phys. A Math. Gen.* **16**, 2993 (1983).
40. N. V. Vitanov, Synthesis of arbitrary SU(*3*) transformations of atomic qutrits. *Phys. Rev. A* **85**, 032331 (2012).
41. A. Celi, P. Massignan, J. Ruseckas, N. Goldman, I. B. Spielman, G. Juzeliūnas, M. Lewenstein, Synthetic gauge fields in synthetic dimensions. *Phys. Rev. Lett.* **112**, 043001 (2014).
42. V. S. Malinovsky, J. L. Krause, General theory of population transfer by adiabatic rapid passage with intense, chirped laser pulses. *Eur. Phys. J. D* **14**, 147–155 (2001).
43. V. G. Arkhipkin, S. A. Myslivets, I. V. Timofeev, Stark-chirped rapid adiabatic passage: Propagation of laser pulses and spacetime evolution of populations and of two-photon coherence. *J. Exp. Theor. Phys.* **97**, 711–721 (2003).
44. R. Bianchetti, S. Filipp, M. Baur, J. M. Fink, C. Lang, L. Steffen, M. Boissonneault, A. Blais, A. Wallraff, Control and tomography of a three level superconducting artificial atom. *Phys. Rev. Lett.* **105**, 223601 (2010).
45. M. Born, V. Fock, Beweis des adiabatensatzes. *Z. Phys.* **51**, 165–180 (1928).
46. M. A. Sillanpää, J. Li, K. Cicak, F. Altomare, J. I. Park, R. W. Simmonds, G. S. Paraoanu, P. J. Hakonen, Autler-Townes effect in a superconducting three-level system. *Phys. Rev. Lett.* **103**, 193601 (2009).
47. J. Li, G. S. Paraoanu, K. Cicak, F. Altomare, J. I. Park, R. W. Simmonds, M. A. Sillanpää, P. J. Hakonen, Decoherence, Autler-Townes effect, and dark states in two-tone driving of a three-level superconducting system. *Phys. Rev. B* **84**, 104527 (2011).

Acknowledgments: This work used the cryogenic facilities of the Low Temperature Laboratory at Aalto University. **Funding:** We acknowledge financial support from FQXi, Väisälä Foundation, the Academy of Finland (project 263457), the Center of Excellence "Low Temperature Quantum Phenomena and Devices" (project 250280), and the "Finnish Center of Excellence in Quantum Technology" (project 312296). **Author contributions:** A.V. and S.D. performed the experiments. S.D. fabricated the sample, and A.V. analyzed the results. A.V. wrote the manuscript together with G.S.P., with additional contributions from S.D. G.S.P. supervised the project. All authors contributed to the planning of the experiments. **Competing interests:** The authors declare that they have no competing interests. **Data and materials availability:** All data needed to evaluate the conclusions in the paper are present in the paper and/or the Supplementary Materials. Additional data related to this paper may be requested from the authors.

Submitted 4 July 2018
Accepted 20 December 2018
Published 8 February 2019
10.1126/sciadv.aau5999

Citation: A. Vepsäläinen, S. Danilin, G. S. Paraoanu, Superadiabatic population transfer in a three-level superconducting circuit. *Sci. Adv.* **5**, eaau5999 (2019).

Superadiabatic population transfer in a three-level superconducting circuit

Antti Vepsäläinen, Sergey Danilin and Gheorghe Sorin Paraoanu

Sci Adv **5** (2), eaau5999.
DOI: 10.1126/sciadv.aau5999